

A Novel Single-Feed Dual-Element Antenna Using Phase Compensation and Magnitude Regulation to Achieve Circular Polarization

Longyue Qu¹, *Member, IEEE*, and Hyeongdong Kim², *Member, IEEE*

Abstract—This paper investigates the design of a novel single-feed dual-element antenna that can be used to achieve circular polarization (CP) performance for mobile devices at arbitrary locations. The severe conditions needed to achieve CP remain as difficult issues for small mobile antennas; this is the case because the ground plane, rather than the antenna structure, contributes to the dominant radiation as the antenna volume shrinks. A novel concept of decomposing the antenna into two elements, which are independently coupled to two orthogonal ground modes for far-field radiation, is proposed through a theoretical analysis based on characteristic mode theory. The proposed dual-element antenna is comprised a loop-type element and monopole-type element, where one element is directly fed and the other resonates parasitically. In this way, the magnitudes and phase difference between two radiated field components can be controlled through antenna tuning without needing to manipulate the ground plane. Both simulations and measurements are conducted to verify the proposed antenna design with a widely used smartphone.

Index Terms—Characteristic mode theory, circular polarization (CP), ground modes, mobile devices, single-feed dual-element antenna.

I. INTRODUCTION

IN WIRELESS communications, signal propagation degrades in harsh environments; using polarization diversity and pattern diversity to improve the channel capacity is necessary for the next-generation communications [1]–[3]. Compared to linearly polarized waves, circularly polarized waves exhibit attractive advantages in terms of their signal propagation, which can overcome multipath interferences and polarization mismatching to obtain better performance [1]–[4]. For these reasons, circularly-polarized waves utilizing two orthogonal, linearly polarized waves can be considered as interesting alternatives to enhance the signal strength and reliability of the overall radio communication link. Circularly polarized antennas have been widely utilized in GPS and satellite communications due to the Faraday rotation when signals penetrate through the ionosphere. In mobile communications, where users are continuously changing their locations with

respect to base stations, the mobility requirement means that circularly polarized antennas are also favorable for maintaining the strength of the received signals of mobile devices, regardless of the orientation.

Circular polarization (CP) can be accomplished under the conditions of two orthogonal modes with equal magnitude and a quadrature phase difference between them; this can be achieved by single-feed and dual-feed methods [5]–[7]. The single-feed method is preferred due to its easy fabrication and low profile; various antenna configurations have been introduced for this method, including microstrip antennas [5]–[11] with various shapes, inserted slots, or diodes; slot/loop antennas [12]–[15]; helical antennas [16]–[19]; crossed dipole antennas [20], [21]; magnetoelectric antennas [22]–[25]; and dielectric resonator antennas [26], [27]. The dual-feed method uses external power dividers for 90° phase generation between two feeds and to allow for their amplitude adjustment [5]–[7]. Moreover, metasurfaces with various artificial structures can operate as polarization converters to manipulate wave polarizations [28]–[32], which have also drawn much attention.

However, in contrast to the aforementioned antennas, mobile antennas must be low profile, miniaturized, and inexpensive, so that they can be integrated onto the platforms of larger ground planes or printed circuit boards (PCBs), whose dimensions are predetermined. Furthermore, the antenna is restricted within a limited volume, and the radiation is dominantly determined by exciting the larger ground plane [33]–[36]. More importantly, a nondirectional radiation pattern is essential due to the communication link with base stations from all directions. For these reasons, all of the above antenna types and metasurfaces are not suitable and/or difficult to implement in mobile devices. Instead, slot-type, loop-type, or monopole-type antennas are typically adopted due to their easy integration, low profile, and low cost [33]–[38].

Furthermore, most previous literature related to mobile antennas focuses on the bandwidth, multiband, and efficiency characteristics, whereas the polarization diversity makes it difficult to satisfy both the magnitude and phase conditions. In [39]–[42], antennas are implemented onto specific rectangular ground planes with intrinsic phase differences between the ground modes; thus, CP can be accomplished by tuning the antenna structures for magnitude regulation. In [43]–[46], manipulation of the ground planes is required to satisfy the phase difference between two orthogonal ground modes for CP generation. However, some of the antenna designs can only be applied to specific cases, and the others

Manuscript received March 20, 2018; revised June 21, 2018; accepted July 8, 2018. Date of publication July 20, 2018; date of current version October 4, 2018. This work was supported by the ICT Research and Development Program of MSIP/IITP, South Korea (ground radiation technique for mobile devices) under Grant 2013-0-00401. (*Corresponding author: Hyeongdong Kim.*)

The authors are with the Department of Electronics and Computer Engineering, Hanyang University, Seoul 04763, South Korea (e-mail: rioinkorea@gmail.com; hdkim@hanyang.ac.kr).

Color versions of one or more of the figures in this paper are available online at <http://ieeexplore.ieee.org>.

Digital Object Identifier 10.1109/TAP.2018.2858180

are larger and more complex due to additional structures on the ground plane. To the best of the authors' knowledge, a comprehensive analysis of CP in mobile devices, as well as a versatile method for small mobile antennas with CP characteristics, has yet to be reported in the literature.

Therefore, this paper focuses on CP generation in mobile antennas, which can be applied at an arbitrary location of an arbitrary ground plane in mobile devices. The proposed single-feed dual-element antenna is composed of a monopole-type element (M-element) and a loop-type element (L-element), where one element is directly excited while the other acts as a parasitic resonator. Section II presents a comprehensive analysis of CP generation in mobile devices. It is important to note that the phase difference between the two orthogonal-radiated fields depends on the intrinsic phase difference between the ground modes. It can also be controlled by utilizing the dual-element antenna technique, so that both the magnitude and phase difference conditions can be satisfied by tuning the antenna without needing to modify the ground plane. In Section III, the proposed technique is first evaluated in a special case using square ground planes with in-phase ground modes (i.e., no intrinsic phase difference between the two orthogonal ground modes). Similar magnitudes are obtained by equally exciting the ground modes along the x -axis and y -axis, while the quadrature phase difference between the two components can be achieved by tuning the resonant frequency of the parasitic element. In Section IV, these dual-element antennas are implemented in a widely used smartphone, where the intrinsic phase difference between the two orthogonal ground modes can compensate for the quadrature phase difference by adopting the proposed dual-element antenna. The axial ratio bandwidth (ARBW) and polarization sense are determined by the intrinsic phase difference and antenna tuning. In this paper, a GPS antenna operating at 1.575 GHz is discussed as a case study.

II. FUNDAMENTAL THEORY

In mobile devices, the antenna elements are much smaller than the ground plane, and the antenna operates as a coupler or exciter to the ground plane. In addition, far-field radiation is generated by the coupling between the antenna element and the ground plane, which has been theoretically and experimentally evaluated in [33]–[36]. Accordingly, excitation of the characteristic modes along the x -axis and y -axis with a proper phase difference yields orthogonal electric field components of \mathbf{E}_x and \mathbf{E}_y along the z -axis, providing CP waves; these can be visualized on the surface of a Poincaré sphere [5]. Generally, this condition for CP generation can be accomplished by two methods.

A. Previous Single-Feed Single-Element Method

The first and most common method is to utilize a single-feed single-element antenna to excite two ground modes simultaneously. Here, the phase differences are basically dependent on the characteristics of the radiative ground plane, which is explained as follows.

Based on characteristic mode theory, the total current distribution \mathbf{J}_t over the surface of a conducting body (e.g., a rectangular ground plane) excited by the antenna can be expressed by the following equations:

$$\mathbf{J}_t = \frac{\iiint (\mathbf{E}_1 \cdot \mathbf{J}_x) d\tau}{1 + j\lambda_x} \cdot \mathbf{J}_x + \frac{\iiint (\mathbf{E}_1 \cdot \mathbf{J}_y) d\tau}{1 + j\lambda_y} \cdot \mathbf{J}_y. \quad (1)$$

Here, \mathbf{E}_1 is the electric field generated by the antenna element only and \mathbf{J}_x and \mathbf{J}_y are the two orthogonal modes in the ground plane. Eigenvalue λ_n is 0 at the resonance of \mathbf{J}_n , and the sign determines whether the mode is inductive ($\lambda_n > 0$) or capacitive ($\lambda_n < 0$) [47]. The relation between the far fields of \mathbf{E}_x and \mathbf{E}_y is represented as

$$\frac{\mathbf{E}_x}{\mathbf{E}_y} = \frac{\iiint (\mathbf{E}_1 \cdot \mathbf{J}_x) d\tau}{\iiint (\mathbf{E}_1 \cdot \mathbf{J}_y) d\tau} \cdot \frac{1 + j\lambda_y}{1 + j\lambda_x}. \quad (2)$$

Here, a single-element antenna is utilized to excite the two ground modes equally to satisfy the magnitude conditions for CP. Accordingly, $\mathbf{E}_x/\mathbf{E}_y = 1e^{\pm i\pi/2}$, i.e., AR = 1, can be obtained by manipulating the resonant frequencies of ground modes \mathbf{J}_x and \mathbf{J}_y (λ_x and λ_y) to be inductive (capacitive) and capacitive (inductive), respectively, at the target frequency. In this way, an intrinsic quadrature phase difference between the ground modes can be provided, whereas the antenna element, operating at the target frequency, determines equal excitation of the ground modes, thereby achieving CP waves. We should note that previous studies of the single-element CP antennas for mobile applications [39]–[46] fall under this case. The situation in mobile antennas, however, is such that the properties of the large ground plane are not easy to control [35], [43]–[46], [48]–[50], which means that the single-element antenna technique is an inefficient and input method for mobile applications.

B. Proposed Single-Feed Dual-Element Method

An alternative method is to construct the antenna out of two coupling elements, which are coupled with each ground mode, so that the desired phase difference can be achieved by controlling the antenna elements without manipulating the ground planes. In this single-feed dual-element antenna technique, the corresponding equation analogous to (1) can be modeled as

$$\mathbf{J}_t = \frac{\iiint (\mathbf{E}_1 \cdot \mathbf{J}_x) d\tau}{1 + j\lambda_x} \cdot \mathbf{J}_x + \frac{\iiint (\mathbf{E}_2 \cdot \mathbf{J}_y) d\tau}{1 + j\lambda_y} \cdot \mathbf{J}_y. \quad (3)$$

Here, \mathbf{E}_1 and \mathbf{E}_2 are the electric fields generated by the dual elements of the antenna, respectively. In this case, each element is dominantly coupled with each ground mode, i.e., there is little coupling between \mathbf{E}_1 and \mathbf{J}_y or between \mathbf{E}_2 and \mathbf{J}_x . Thus, the relation between the far fields of \mathbf{E}_x and \mathbf{E}_y becomes

$$\frac{\mathbf{E}_x}{\mathbf{E}_y} = \frac{\iiint (\mathbf{E}_1 \cdot \mathbf{J}_x) d\tau}{\iiint (\mathbf{E}_2 \cdot \mathbf{J}_y) d\tau} \cdot \frac{1 + j\lambda_y}{1 + j\lambda_x}. \quad (4)$$

Accordingly, the magnitude conditions for CP can be fulfilled by controlling the dual elements to equally excite both two ground modes (\mathbf{J}_x and \mathbf{J}_y). Furthermore, the dual-element antenna must generate a desired phase difference to

compensate the intrinsic phase difference between the ground modes, thereby satisfying the total quadrature phase difference. It is noted that the desired phase difference generated by the dual-element antenna can be obtained by tuning the dual elements (E_1 and E_2) at different resonant frequencies, while the intrinsic phase difference between the ground modes is dependent on the resonant frequencies of the ground modes (λ_x and λ_y). Consequently, both the intrinsic phase difference between ground modes and the phase difference provided by the dual-element antenna can determine the total phase difference between E_x and E_y . Accordingly, the polarization sense will then be determined by both the antenna and the ground plane. Therefore, different from the single-feed single-element method, the proposed dual-element method utilizes only antenna elements to control the magnitude and phase conditions, regardless of the resonances of the ground modes.

In a special and simplified case, where both ground modes have identical resonant frequencies, i.e., there is no intrinsic phase difference between the two ground modes, (4) is simplified as

$$\frac{E_x}{E_y} = \frac{\iiint (\mathbf{E}_1 \cdot \mathbf{J}_x) d\tau}{\iiint (\mathbf{E}_2 \cdot \mathbf{J}_y) d\tau}. \quad (5)$$

Accordingly, the quadrature phase difference can be fulfilled by manipulating E_1 and E_2 without considering the ground modes, and the polarization sense will be determined by the phases of E_1 and E_2 . This case can be easily understood by considering the dual-feed method for microstrip antennas, where two feeds are fed in such a way that a 90° time-phase difference is provided [5]–[7].

In this way, the dual-element technique is expected to be a better and more efficient method in antenna-ground systems; CP can be achieved by the antenna element without manipulating the ground plane, which is an important issue that has not yet been discussed in the literature. This is first discussed in a special case with a square ground plane and then applied to a general case with a rectangular ground plane.

III. ANTENNA CONFIGURATIONS IN THE SPECIAL CASE OF A SQUARE GROUND PLANE

A. Antenna Implementation

Implementation of the proposed dual-element antennas with CP is initially demonstrated in a square ground plane ($60 \text{ mm} \times 60 \text{ mm}$), where the intrinsic phase difference between the two ground modes can be ignored; thus, the quadrature time-phase difference between the two orthogonal far-field components can be obtained by only tuning the antenna elements, as indicated in (5).

Fig. 1 depicts the configuration of the proposed dual-element antenna, which is comprised a capacitively fed L-element and a parasitic M-element. For simplicity, the M-element, with horizontal length l (20 mm), is loaded with a series inductor L (11.7 nH) at the current maximum portions of the M-element, so that the inductor values can be easily tuned to control the resonant frequency of the M-element. The L-element ($4 \text{ mm} \times 8 \text{ mm}$) is excited through

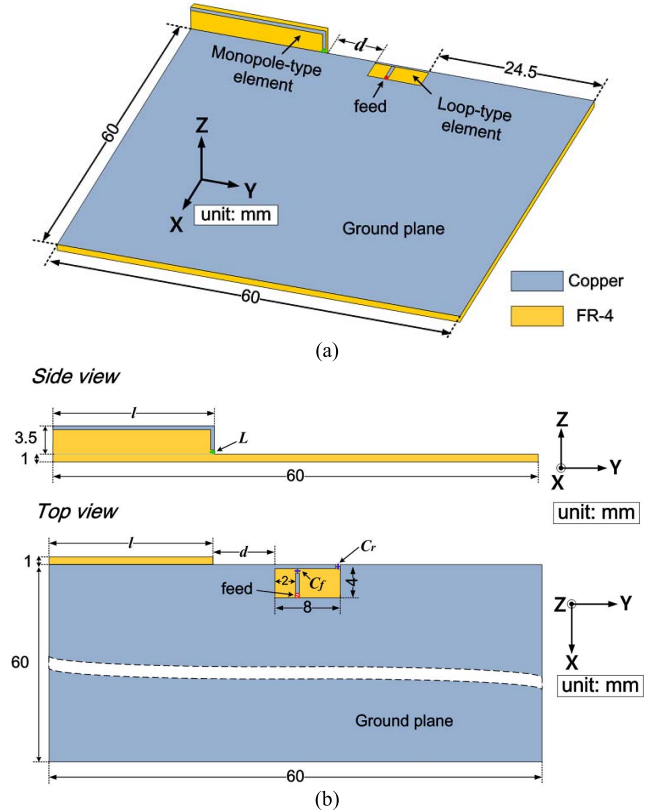


Fig. 1. Antenna configurations of the proposed dual-element antenna in a square ground plane. (a) Elevation view and (b) side view of the M-element and top view of the L-element.

capacitor C_f (0.7 pF) for input impedance matching, while capacitor C_r (0.7 pF) is connected to a conductor line at the open portions of the ground clearance, forming a loop-type resonator with convenient control of its resonant frequency by adjusting the capacitor values [36], [45], [51]–[54]. The edge-to-edge distance between the two elements is $d = 7.5 \text{ mm}$, and the width of all the conductor lines is set as 0.5 mm . More detailed dimensions can be found in Fig. 1.

Fig. 2(a) presents the simulated results of the reflection coefficient and the AR values generated by the proposed dual-element antenna. The 3:1 VSWR bandwidth covers 90 MHz (from 1.51 to 1.60 GHz), and a 3 dB ARBW of 20 MHz (from 1.565 to 1.585 GHz) is produced along the z -axis. Fig. 2(b) shows the polarization patterns in the xz plane at 1.575 GHz. It can be observed that left-hand circular polarization (LHCP) and right-hand CP (RHCP) are generated in the $+z$ -direction and $-z$ -direction, respectively. The circularly polarized waves are formed by the orthogonal electric field components E_x and E_y , which contribute by exciting dominant modes along the x -axis and y -axis of the ground plane (\mathbf{J}_x and \mathbf{J}_y), respectively.

The operation mechanisms are introduced as follows.

The proposed antenna can be optimized by first setting the capacitively fed L-element at an arbitrary location (operating at the target frequency band) and then inserting the parasitic M-element for the purpose of equal magnitude and quadrature phase difference. As can be observed from the impedance locus in the Smith chart of Fig. 3, dual resonant

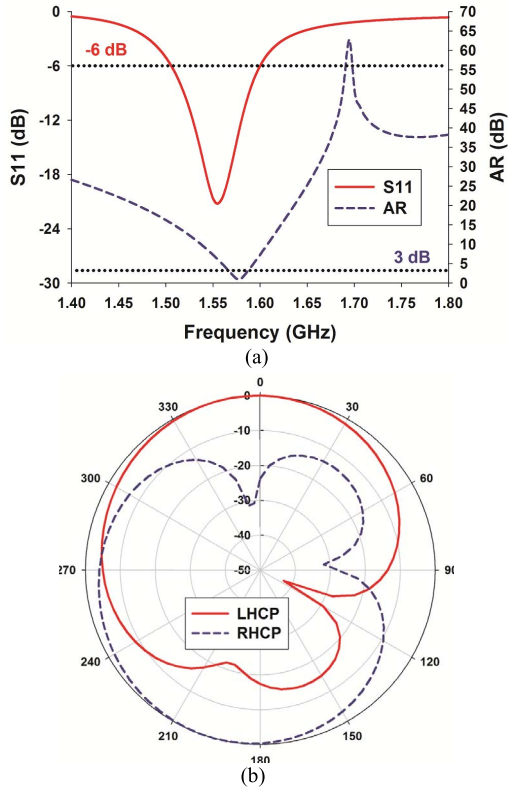


Fig. 2. Simulated results. (a) Reflection coefficient and AR values ($\varphi = 0$ and $\theta = 0$) and (b) normalized polarization patterns in the xz plane at 1.575 GHz.

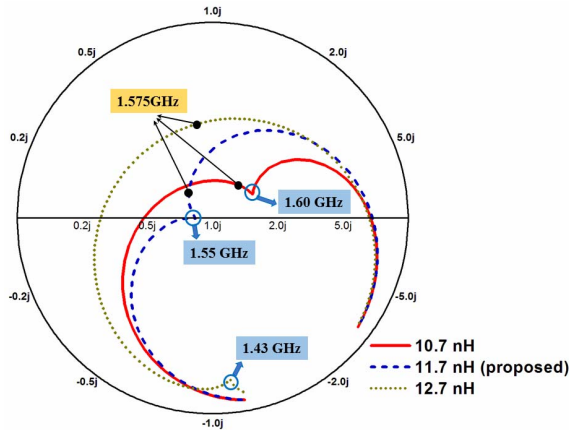


Fig. 3. Input impedance in a Smith chart with variations in the inductor value of L .

modes are generated by the proposed dual-element antenna. The capacitively fed L-element produces the larger impedance locus by coupling with ground mode J_y , i.e., $\iiint (\mathbf{E}_2 \cdot \mathbf{J}_y) d\tau$, and its resonant frequency is directly determined by the loop size and capacitor value (C_r) of the L-element. The parasitic M-element, coupled with ground mode J_x by $\iiint (\mathbf{E}_1 \cdot \mathbf{J}_x) d\tau$, introduces the smaller parasitic impedance locus at a frequency slightly below 1.575 GHz, and its resonant frequency is dominantly controlled by the length and inductor value (L) of the M-element. Dual resonant modes of the proposed dual-element antenna allow equal amplitudes of two ground modes with quadrature phase difference to be excited at an arbitrary location in the ground plane.

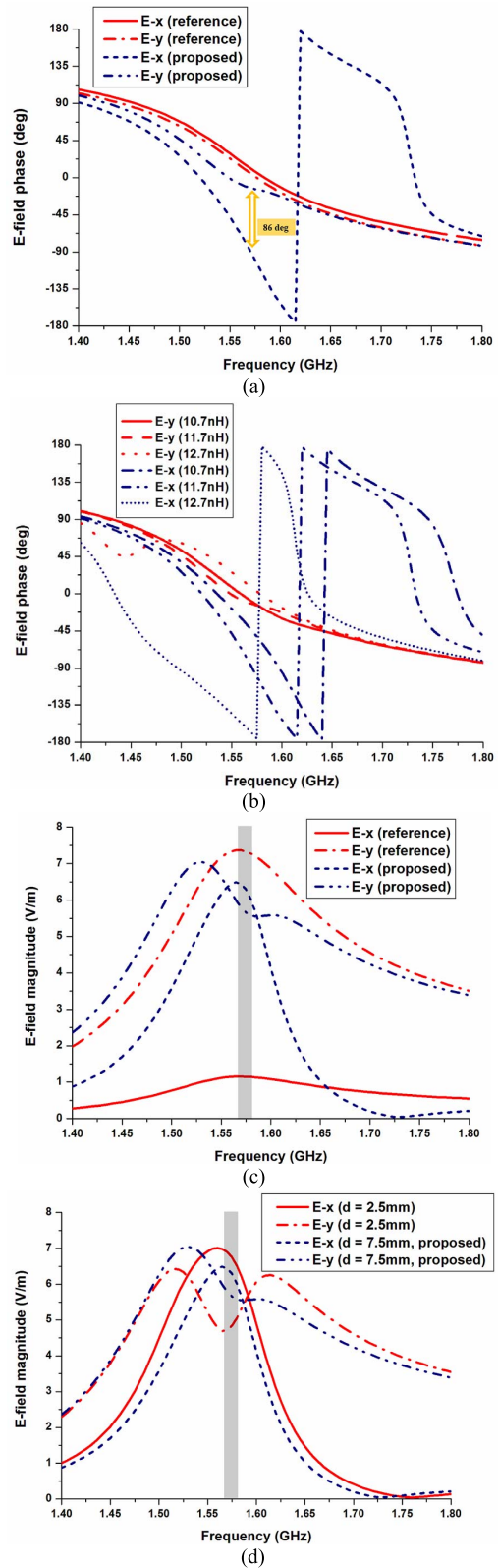


Fig. 4. Simulated results of the far fields of E_x and E_y ($\varphi = 0$ and $\theta = 0$). (a) Phase, (b) phase variation with different values of L , (c) magnitude, and (d) magnitude variation with different values of d .

In Fig. 4(a), the simulated results of the far fields E_x and E_y in the $+z$ -direction are shown. Without utilization of the M-element, the two components are almost in-phase without

a phase difference; this is due to the identical resonant frequencies of the two ground modes. In the proposed design, it can be observed that E_x is delayed while E_y is almost constant, resulting in an 86° phase difference. When the resonant frequency of the M-element is lowered by increasing the inductor value from 9.7 to 12.7 nH, the phase delay of the E_x component relative to E_y is increased from 38° to 178° , as can be verified in Fig. 4(b). Meanwhile, the variation of the impedance characteristics can also be verified by observing the smaller locus in the Smith chart of Fig. 3, which rotates in the counterclockwise direction. Therefore, it is obvious that the phase of the E_x component is greatly dependent on the variation of the resonant frequency of the M-element; this enables the phase difference between the two field components to be easily controlled. Note that a rapid change in the phase difference occurs as a function of the frequency due to the high quality factor (Q) of the M-element, which is consistent with the narrow ARBW. Herein, one effective way to improve ARBW can be expected by controlling the E_x component slowly changed with frequency in both phase and magnitude; this can be realized by, for example, designing the M-element as an electrically larger one.

Moreover, the parasitic M-element also plays an important role in magnitude regulation between the two components. It is well known that the L-element works as a magnetic coupler to ground mode J_y , while the M-element works as an electric coupler to ground mode J_x ; thus, dual elements are necessary for magnitude regulation between E_x and E_y in order to obtain equal excitation of both ground modes. As can be seen from Fig. 4(c), the L-element can only excite E_y dominantly, in which case the antenna corresponds to a conventional ground radiation antenna [36], [45], [51]–[54]; however, with the adoption of the M-element, half of the energy is coupled to the M-element and ground mode J_x , contributing to the enhanced value of E_y . It is important to note that the magnitude regulation depends on the coupling between the two elements, as well as on the coupling between each element and the ground mode, which can be adjusted by changing the distance between the two elements or by modifying the element volumes. Here, the magnitude variation with the edge-to-edge distance (d) between the two elements is briefly discussed in Fig. 4(d), where the data are obtained by moving the M-element closer to the L-element. Decreased E_y component and increased E_x component can be observed as d is changed from 7.5 to 2.5 mm, so that their magnitude difference becomes wider at the target frequency. Therefore, the distance between the two elements can be adjusted to conveniently control the coupled energy from the L-element to the parasitic M-element, further contributing to the magnitude regulation.

To verify the proposed dual-element antenna, the simulated surface current distributions at 1.575 GHz are plotted in Fig. 5. The current paths over the antenna elements are first investigated in Fig. 5(a), and it can be clearly observed that a monopole-type current path (dashed arrow line) and a loop-type current path (solid arrow line) are simultaneously generated over the M-element and L-element, respectively, which is in accordance with the dual resonant modes of the proposed antenna. Since the antenna elements act as couplers

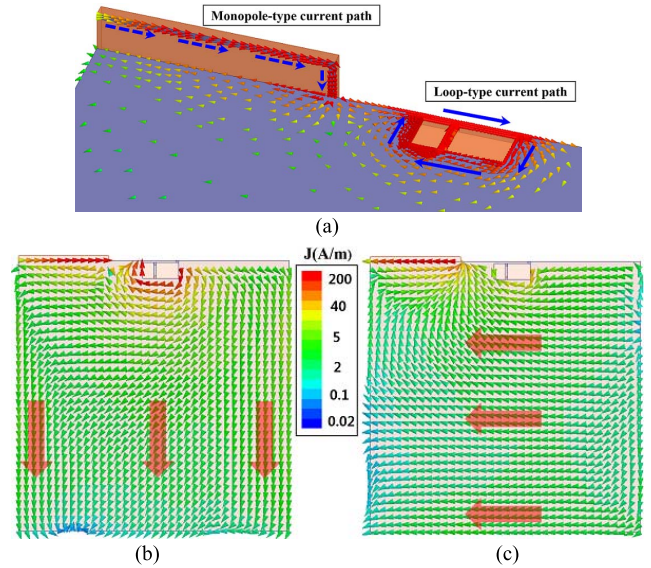


Fig. 5. Simulated surface current distributions. (a) Current paths over the antenna elements. (b) Current flow over the ground plane at $t = 0$. (c) Current flow over the ground plane at $t = T/4$.

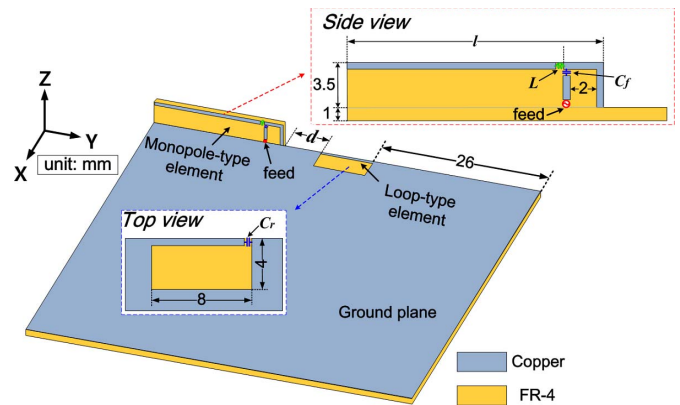


Fig. 6. Alternative antenna configuration.

to the ground modes of the ground plane as real radiators, the current flow over the ground plane should be observed in time period T . At $t = 0$, the current distributions over the ground plane flow along the $+x$ -direction, as can be observed in Fig. 5(b). Alternatively, at $t = T/4$, the current flows along the $-y$ -direction in Fig. 5(c). The time period-based current movements are consistent with the polarization sense, as discussed above. It can be concluded that the current paths over the high- Q antenna elements can determine the antenna's dual resonant frequencies, while the current flows along the low- Q ground modes excited by the antenna elements are contributing to the CP radiation, regardless of the resonances of the ground modes.

B. Antenna Design With Reverse Polarization Sense

Alternatively, the proposed dual-element antenna can be implemented by utilizing a capacitively fed M-element and a parasitic L-element to produce reversed polarization senses.

The antenna configuration is depicted in Fig. 6. The M-element is fed through capacitor C_f (1 pF) for impedance matching, and series inductor L (13.5 nH) is loaded at the

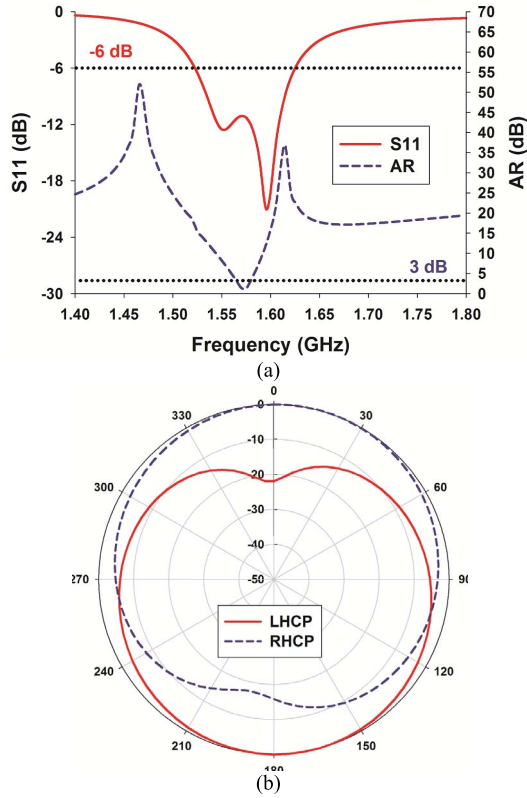


Fig. 7. Simulated results. (a) Reflection coefficient and AR values ($\varphi = 0$ and $\theta = 0$). (b) Normalized polarization radiation pattern in the xz plane at 1.575 GHz.

portions where strong currents are flowing over the M-element, so that its resonant frequency can be easily adjusted by tuning the inductor values. In addition, to ensure independent control of the resonant frequency without affecting the impedance matching, inductor L is located outside of the feeding structure (left side of capacitor C_f). Similar to Fig. 1, the resonant frequency of the parasitic L-element can be tuned by capacitor C_r (0.85 pF) without changing the loop size. Other relevant parameters are $d = 6$ mm and $l = 20$ mm.

The simulated results are briefly described below. The 3:1 VSWR bandwidth covers from 1.53 to 1.63 GHz and the ARBW is from 1.57 to 1.58 GHz, as can be seen from Fig. 7(a). The polarization radiation patterns in Fig. 7(b) are opposite to those in Fig. 2(b); this is the case because the L-element operates as a parasitic resonator at lower frequency, providing the phase-lagging component E_y . As can be verified from the input impedance locus in Fig. 8(a), the M-element and the parasitic L-element produce the larger locus and the smaller locus in the Smith chart, respectively, generating dual resonant modes. The corresponding magnitudes and phases of the far-field components of E_x and E_y can be confirmed in Fig. 8(b); equal magnitudes and 83° phase delay of E_y to E_x can be observed, which are in accordance with the input impedance locus and the polarization sense.

Furthermore, the surface current distributions over the ground plane in time period T are demonstrated in Fig. 9. It can be observed that the current distributions are directed

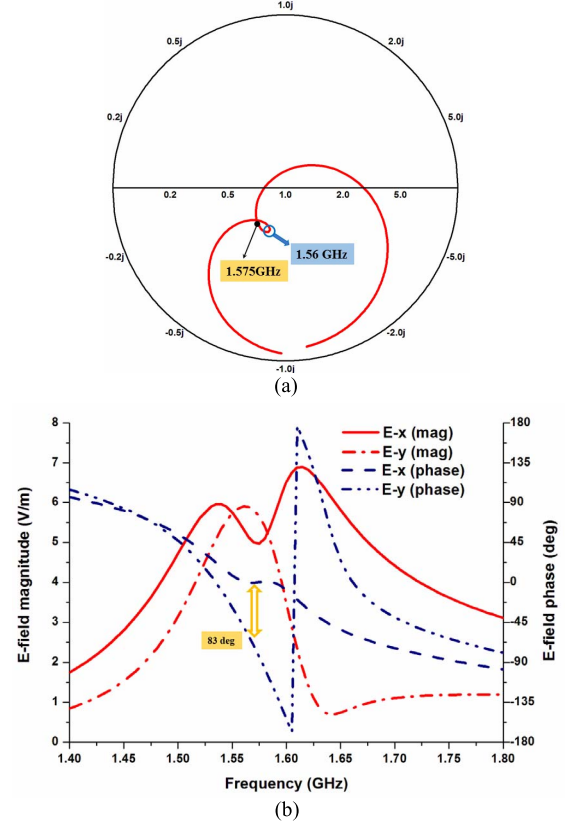


Fig. 8. Simulated results. (a) Input impedance in a Smith chart and (b) phases and magnitudes of far fields E_x and E_y ($\varphi = 0$ and $\theta = 0$).

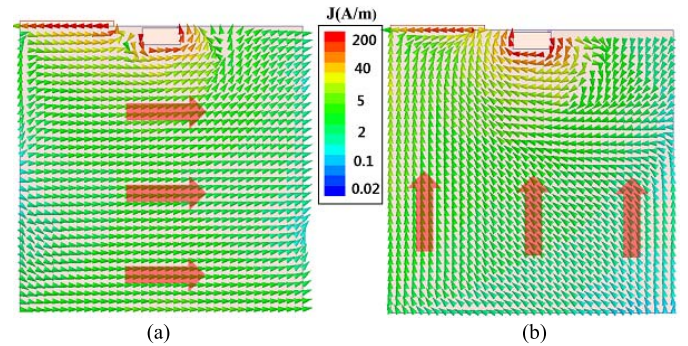


Fig. 9. Simulated surface current distributions over the ground plane at (a) $t = 0$ and (b) $t = T/4$.

along the $+y$ -direction at $t = 0$ and in the $-x$ -direction at $t = T/4$. The current movement in time period T changes according to the polarization sense of the proposed antenna. Therefore, the CP performance with optional polarization sense can be provided by manipulating E_1 and E_2 of the two elements in the proposed dual-feed antenna, as derived from (5).

IV. DEMONSTRATION IN MOBILE DEVICE APPLICATIONS

In a rectangular ground plane, which is the case used for most mobile devices, the intrinsic phase difference between the ground modes should be considered, as indicated in (4).

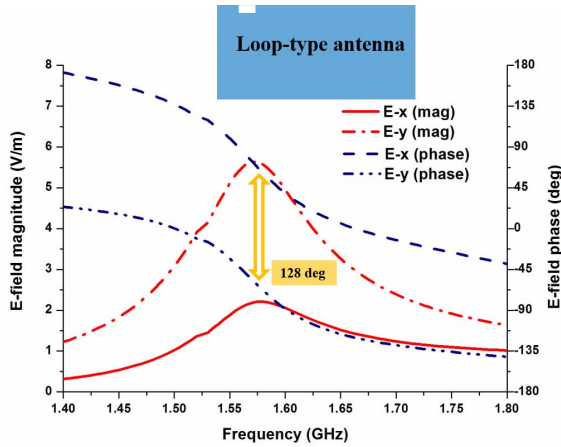


Fig. 10. Phases and magnitudes of far fields E_x and E_y generated by the L-element only ($\varphi = 0$ and $\theta = 0$).

Accordingly, the proposed dual-element antenna is adopted to provide the desired phase compensation for the intrinsic phase difference to deliver a quadrature phase difference. Therefore, the proposed technique is evaluated in a $70 \text{ mm} \times 140 \text{ mm}$ ground plane by using the capacitively fed L-element and parasitic M-element.

To start, a reference L-element antenna without the parasitic M-element is discussed. As can be seen from Fig. 10, the loop-type antenna dominantly excites E_y . Meanwhile, E_x is leading by 128° relative to E_y at the target frequency band; this is due to the fact that the dominant ground mode along the x -axis (J_x) resonates at a frequency higher than the dominant ground mode along the y -axis (J_y). According to (4), phase compensation for the intrinsic phase difference between the two ground modes is required to satisfy the quadrature phase difference. This can occur by more than one method:

- 1) lagging E_x with phase compensation of 38° (i.e., E_x leads E_y by 90°);
- 2) lagging E_x with phase compensation of 218° (i.e., E_x lags E_y by 90°).

Both methods can provide CP performance but with opposite polarization senses. Therefore, in Sections IV-A and IV-B, each possible solution is demonstrated with the proposed antenna. Furthermore, it is important to note that though the proposed dual-element antenna is discussed in a $70 \text{ mm} \times 140 \text{ mm}$ platform for the case study, it can be applicable to various mobile devices with different dimensions, since the dimensions only contribute to the intrinsic phase difference between the two ground modes [see (4)]. Corresponding tuning can be necessary to optimize the CP performance for applications in various devices.

A. Solution (a)

To demonstrate the first potential solution, the parasitic M-element is introduced to tune the E_x component in order to make E_x lead E_y by 90° . The configuration of the proposed antenna and its fabricated prototype are shown in Fig. 11.

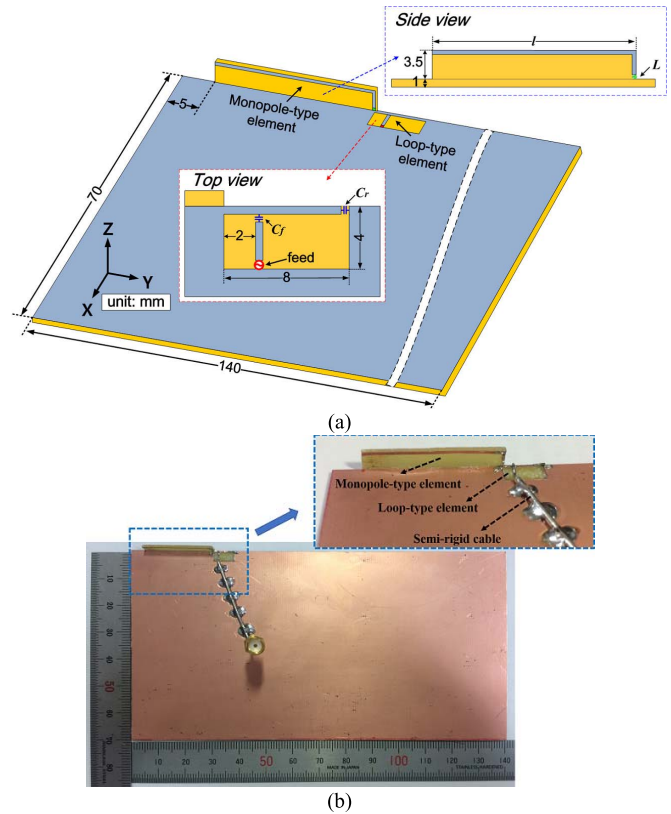


Fig. 11. Proposed dual-element antenna with the first solution. (a) Configuration and (b) prototype of the fabricated antenna.

The optimized parameters are listed as $C_f = 0.7 \text{ pF}$, $C_r = 0.68 \text{ pF}$, $l = 25 \text{ mm}$, $L = 3.5 \text{ nH}$, and $d = 0 \text{ mm}$.

As expected and shown in Fig. 12(a), the phase of the E_x component is delayed by 45° compared with the reference results of Fig. 9, while the E_y component is barely affected. Furthermore, the magnitude of the E_x component is greatly improved, resulting in similar amplitudes for both field components. The optimized results can be obtained by first tuning the resonant frequency of the parasitic M-element to adjust the phase difference, and then by modifying the distance between the two elements to regulate the magnitudes. It is interesting to observe that the slope of the phase difference smoothly changes as a function of the frequency, which is significantly different from the results obtained in the square ground plane. This difference can be explained by the fact that the resonant frequency of the parasitic M-element falls at a frequency that is further away from the target frequency, which can be confirmed based on the smaller parasitic impedance locus in Fig. 12(b). Accordingly, the smooth slope is dominantly attributed to the low- Q ground modes.

Fig. 13 shows the simulated and measured results of the proposed antenna design. The antenna covers a bandwidth of 80 MHz (from 1.54 to 1.62 GHz) in the simulation, and a parasitic resonance can be observed at the higher frequency band, which is generated by the M-element. As expected, a wideband ARBW of 120 MHz (from 1.50 to 1.62 GHz) is observed due to the smooth slope of the phase difference.

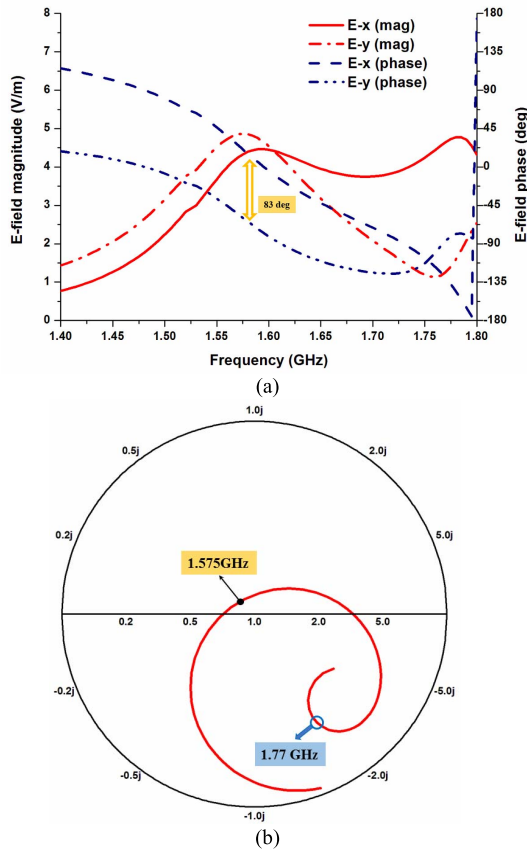


Fig. 12. Simulated results. (a) Phases and magnitudes of far fields E_x and E_y ($\varphi = 0$ and $\theta = 0$) and (b) input impedance in a Smith chart.

In addition, the proposed antenna produces RHCP and LHCP in the $+z$ - and $-z$ -directions, respectively, as shown in the xz plane of Fig. 13(b). The CP radiation in the upper hemisphere generated by the proposed dual-element antenna can be particularly attractive to the navigation requirement for mobile devices [39], [40], [42], [44]. Note that the asymmetric radiation patterns result from the higher mode along the y -axis of the ground plane. The measured efficiency at 1.575 GHz is 72% with a peak gain of 3 dBi, indicating the high performance of the proposed antenna. It can be concluded that the simulated and measurement results agree with each other. In real application scenarios, high-speed digital-integrated circuits along with various components are etched onto the PCB to achieve multifunctionality, and noise emitted from these circuits can bring electromagnetic interference to the victim antennas; this is another important issue for antenna engineers, and several potential solutions for different kinds of antenna types can be found in [54]–[56].

B. Solution (b)

The other potential solution is presented by providing more phase delay to the E_x component so that E_x lags E_y by 90° . According to the results in Fig. 2(b), the parasitic resonance of the M-element should be tuned lower than that in Fig. 12. The optimized antenna design shown in Fig. 14(a) is the same as that in Fig. 11(a), but with a different edge-to-edge

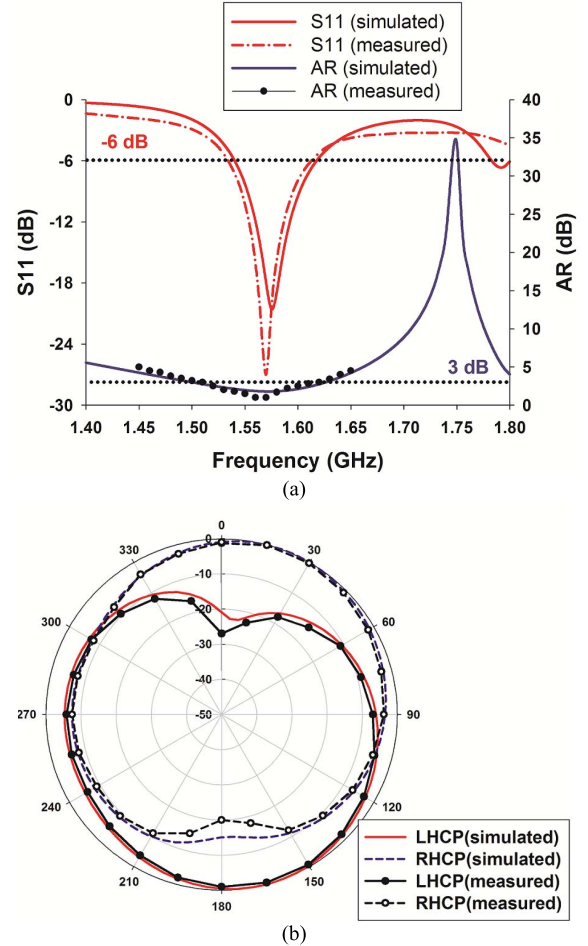


Fig. 13. Simulated and measured results. (a) Reflection coefficients and AR values ($\varphi = 0$ and $\theta = 0$) and (b) normalized polarization patterns in the xz plane at 1.575 GHz.

distance d (6 mm) caused by shifting the M-element to the left side. The optimized parameters are set as $C_f = 0.75$ pF, $C_r = 0.75$ pF, and $L = 7.4$ nH. The fabricated prototype is also shown in Fig. 14(b) for verification.

Fig. 15(a) presents the magnitudes and phases of the far fields in simulation. By tuning the resonant frequency of the parasitic M-element, the phase of E_x is tuned to lag E_y by 85° , without greatly affecting E_y . Furthermore, after adopting the M-element, the magnitude of E_x is approximately excited to be equal to that of E_y . In this case, the resonant frequency of the M-element is near the target frequency [slightly lower than the target frequency, as shown in Fig. 15(b)], such that the phase of E_x varies quickly with frequency; this is dominantly determined by the high- Q M-element, resulting in the steep slope of the phase difference.

The simulated and measured results are shown in Fig. 16. The impedance bandwidth covers a wideband of 1.49 to 1.60 GHz due to the dual resonant modes, while the ARBW is 20 MHz (from 1.57 to 1.59 GHz). It can be observed that the ARBW is narrowband, similar to the cases in the square ground plane. This is the case because the phase difference between the two field components is greatly

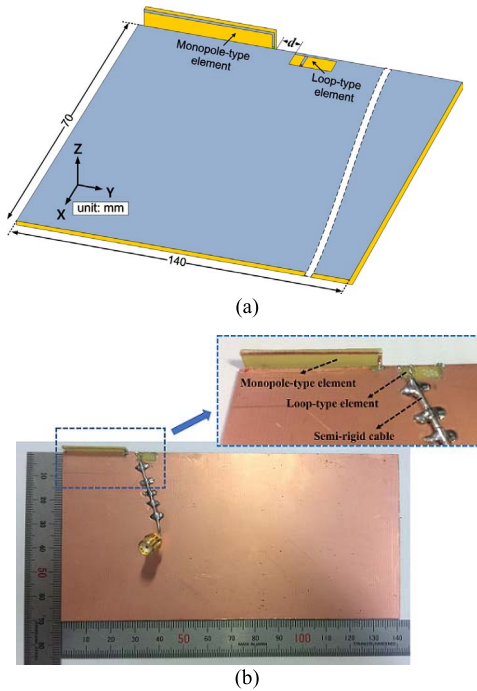


Fig. 14. Proposed dual-element antenna for an alternative solution. (a) Configuration. (b) Fabrication.

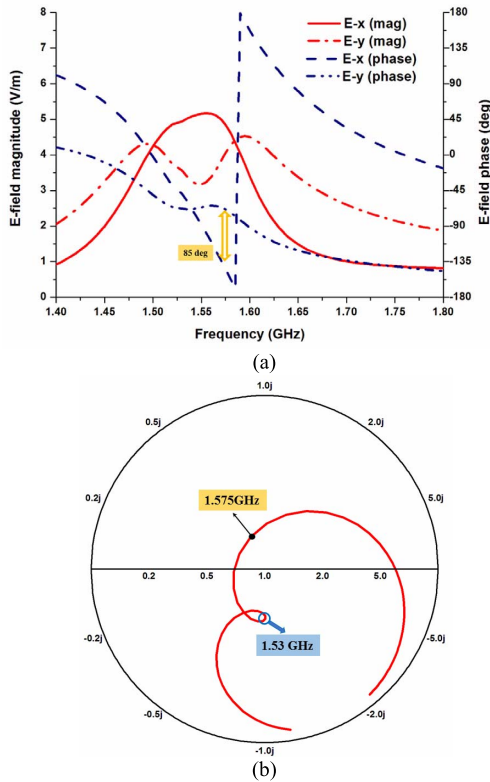


Fig. 15. Simulated results. (a) Phase and magnitude of far fields E_x and E_y ($\varphi = 0$ and $\theta = 0$). (b) Input impedance in a Smith chart.

affected by the characteristics of the M-element (instead of by the ground mode). In Fig. 16(b), the polarization senses are opposite to those in Fig. 13(b), providing LHCP and

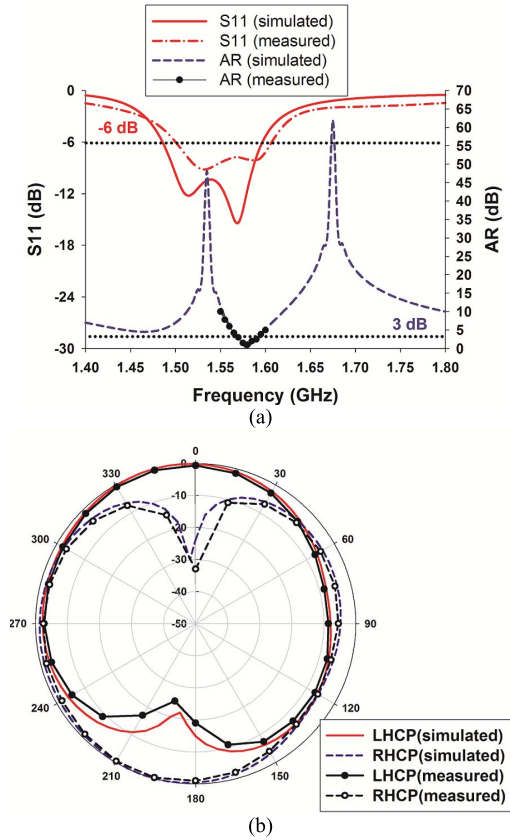


Fig. 16. Simulated and measured results. (a) Reflection coefficients and AR values ($\varphi = 0$ and $\theta = 0$). (b) Normalized polarization patterns in the xz plane at 1.575 GHz.

RHCP in the $+z$ - and $-z$ -directions, respectively. It is noted that the measured total efficiency at 1.575 GHz is 60% with a peak gain of 2.4 dBi, and the simulation and measurement results agree well with each.

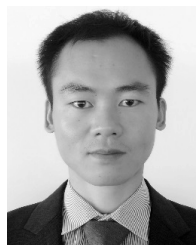
V. CONCLUSION

A dual-element antenna consisting of an M-element and an L-element is proposed as a versatile method to provide CP performance at arbitrary locations of mobile devices. It has been shown that the phase difference of the far-field components is dependent on the intrinsic characteristics of the ground modes and can be controlled by manipulating the antenna elements. Therefore, the proposed antenna design can equally excite two orthogonal ground modes for radiation with the same magnitudes by adopting two coupling elements. It can also provide the desired phase difference between two orthogonal field components by tuning the resonant frequency of the parasitic element. In addition, alternative polarization senses can be achieved by controlling the two elements, irrespective of the characteristics of the ground modes. Furthermore, a wide ARBW can be obtained by providing phase compensation for the intrinsic phase difference of the ground modes in a rectangular ground plane, in which the polarization sense is determined by the ground plane. Therefore, the proposed antenna technique can be applied to mobile devices for CP applications.

REFERENCES

- [1] R. G. Vaughan, "Polarization diversity in mobile communications," *IEEE Trans. Veh. Technol.*, vol. 39, no. 3, pp. 177–186, Aug. 1990.
- [2] C. B. Dietrich, K. Dietze, J. R. Nealy, and W. L. Stutzman, "Spatial, polarization, and pattern diversity for wireless handheld terminals," *IEEE Trans. Antennas Propag.*, vol. 49, no. 9, pp. 1271–1281, Sep. 2001.
- [3] P. Mattheijssen, M. H. A. J. Herben, G. Dolmans, and L. Leyten, "Antenna-pattern diversity versus space diversity for use at handhelds," *IEEE Trans. Veh. Technol.*, vol. 53, no. 4, pp. 1035–1042, Jul. 2004.
- [4] F. A. Dicandia, S. Genovesi, and A. Monorchio, "Analysis of the performance enhancement of MIMO systems employing circular polarization," *IEEE Trans. Antennas Propag.*, vol. 65, no. 9, pp. 4824–4835, Sep. 2017.
- [5] C. A. Balanis, *Antenna Theory: Analysis and Design*, 4th ed. Hoboken, NJ, USA: Wiley, 2016.
- [6] R. Garg, P. Bhartia, I. J. Bahl, and A. Ittipiboon, *Microstrip Antenna Design Handbook*. Norwood, MA, USA: Artech House, 2001.
- [7] S. S. Gao, Q. Luo, and F. Zhu, *Circularly Polarized Antennas*. Hoboken, NJ, USA: Wiley, 2014.
- [8] J. Y. Jan, C. Y. Pan, K. Y. Chiu, and H. M. Chen, "Broadband CPW-fed circularly-polarized slot antenna with an open slot," *IEEE Trans. Antennas Propag.*, vol. 61, no. 3, pp. 1418–1422, Mar. 2013.
- [9] K. F. Tong and T. P. Wong, "Circularly polarized U-slot antenna," *IEEE Trans. Antennas Propag.*, vol. 55, no. 8, pp. 2382–2385, Aug. 2007.
- [10] C.-J. Wang and W.-B. Tsai, "Microstrip open-slot antenna with broadband circular polarization and impedance bandwidth," *IEEE Trans. Antennas Propag.*, vol. 64, no. 9, pp. 4095–4098, Sep. 2016.
- [11] P.-Y. Qin, A. R. Weily, Y. J. Guo, and C.-H. Liang, "Polarization reconfigurable U-slot patch antenna," *IEEE Trans. Antennas Propag.*, vol. 58, no. 10, pp. 3383–3388, Oct. 2010.
- [12] K.-L. Wong, C.-C. Huang, and W.-S. Chen, "Printed ring slot antenna for circular polarization," *IEEE Trans. Antennas Propag.*, vol. 50, no. 1, pp. 75–77, Jan. 2002.
- [13] W. Lei, H. Chu, and Y.-X. Guo, "Design of a circularly polarized ground radiation antenna for biomedical applications," *IEEE Trans. Antennas Propag.*, vol. 64, no. 6, pp. 2535–2540, Jun. 2016.
- [14] W.-T. Hsieh, T.-H. Chang, and J.-F. Kiang, "Dual-band circularly polarized cavity-backed annular slot antenna for GPS receiver," *IEEE Trans. Antennas Propag.*, vol. 60, no. 4, pp. 2076–2080, Apr. 2012.
- [15] R. L. Li, B. Pan, A. N. Traille, J. Papapolymerou, J. Laskar, and M. M. Tentzeris, "Development of a cavity-backed broadband circularly polarized slot/strip loop antenna with a simple feeding structure," *IEEE Trans. Antennas Propag.*, vol. 56, no. 2, pp. 312–318, Feb. 2008.
- [16] C. Liu, Y.-X. Guo, and S. Xiao, "Circularly polarized helical antenna for ISM-band ingestible capsule endoscopy systems," *IEEE Trans. Antennas Propag.*, vol. 62, no. 12, pp. 6027–6039, Dec. 2014.
- [17] Z. Chen and Z. Shen, "Planar helical antenna of circular polarization," *IEEE Trans. Antennas Propag.*, vol. 63, no. 10, pp. 4315–4323, Oct. 2015.
- [18] X. Tang, Y. He, and B. Feng, "Design of a wideband circularly polarized strip-helical antenna with a parasitic patch," *IEEE Access*, vol. 4, pp. 7728–7735, 2016.
- [19] C. Morlaas, B. Souny, and A. Chaborry, "Helical-ring antenna for hemispherical radiation in circular polarization," *IEEE Trans. Antennas Propag.*, vol. 63, no. 11, pp. 4693–4701, Nov. 2015.
- [20] Y.-X. Sun, K. W. Leung, and K. Lu, "Broadbeam cross-dipole antenna for GPS applications," *IEEE Trans. Antennas Propag.*, vol. 65, no. 10, pp. 5605–5610, Oct. 2017.
- [21] W.-S. Yoon, S.-M. Han, J.-W. Baik, S. Pyo, J. Lee, and Y.-S. Kim, "Crossed dipole antenna with switchable circular polarisation sense," *Electron. Lett.*, vol. 45, no. 14, pp. 717–718, Jul. 2009.
- [22] W. Lin and R. W. Ziolkowski, "Electrically small, low-profile, Huygens circularly polarized antenna," *IEEE Trans. Antennas Propag.*, vol. 66, no. 2, pp. 636–643, Feb. 2018.
- [23] F. Wu and K.-M. Luk, "Wideband tri-polarization reconfigurable magneto-electric dipole antenna," *IEEE Trans. Antennas Propag.*, vol. 65, no. 4, pp. 1633–1641, Apr. 2017.
- [24] Y. Li and K.-M. Luk, "A 60-GHz wideband circularly polarized aperture-coupled magneto-electric dipole antenna array," *IEEE Trans. Antennas Propag.*, vol. 64, no. 4, pp. 1325–1333, Apr. 2016.
- [25] K. Kang, Y. Shi, and C.-H. Liang, "A wideband circularly polarized magneto-electric dipole antenna," *IEEE Antennas Wireless Propag. Lett.*, vol. 16, pp. 1647–1650, 2017.
- [26] L. Guo and K. W. Leung, "Compact unilateral circularly polarized dielectric resonator antenna," *IEEE Trans. Antennas Propag.*, vol. 66, no. 2, pp. 668–674, Feb. 2018.
- [27] Z. Chen and H. Wong, "Liquid dielectric resonator antenna with circular polarization reconfigurability," *IEEE Trans. Antennas Propag.*, vol. 66, no. 1, pp. 444–449, Jan. 2018.
- [28] H. L. Zhu, S. W. Cheung, K. L. Chung, and T. I. Yuk, "Linear-to-circular polarization conversion using metasurface," *IEEE Trans. Antennas Propag.*, vol. 61, no. 9, pp. 4615–4623, Sep. 2013.
- [29] H. L. Zhu, S. W. Cheung, X. H. Liu, and T. I. Yuk, "Design of polarization reconfigurable antenna using metasurface," *IEEE Trans. Antennas Propag.*, vol. 62, no. 6, pp. 2891–2898, Jun. 2014.
- [30] W. Li *et al.*, "A reconfigurable polarization converter using active metasurface and its application in horn antenna," *IEEE Trans. Antennas Propag.*, vol. 64, no. 12, pp. 5281–5290, Dec. 2016.
- [31] W. Li *et al.*, "Polarization-reconfigurable circularly polarized planar antenna using switchable polarizer," *IEEE Trans. Antennas Propag.*, vol. 65, no. 9, pp. 4470–4477, Sep. 2017.
- [32] F. F. Farzami, S. Khaledian, B. Smida, and D. Erricolo, "Reconfigurable linear/circular polarization rectangular waveguide filter," *IEEE Trans. Antennas Propag.*, vol. 66, no. 1, pp. 9–15, Jan. 2018.
- [33] J. Villanen, J. Ollikainen, O. Kivekas, and P. Vainikainen, "Coupling element based mobile terminal antenna structures," *IEEE Trans. Antennas Propag.*, vol. 54, no. 7, pp. 2142–2153, Jul. 2006.
- [34] P. Vainikainen, J. Ollikainen, O. Kivekas, and I. Kelder, "Resonator-based analysis of the combination of mobile handset antenna and chassis," *IEEE Trans. Antennas Propag.*, vol. 50, no. 10, pp. 1433–1444, Oct. 2002.
- [35] L. Qu, R. Zhang, H. Shin, J. Kim, and H. Kim, "Mode-controlled wideband slot-fed ground radiation antenna utilizing metal loads for mobile applications," *IEEE Trans. Antennas Propag.*, vol. 65, no. 2, pp. 867–872, Feb. 2017.
- [36] L. Qu, R. Zhang, and H. Kim, "Decoupling between ground radiation antennas with ground-coupled loop-type isolator for WLAN applications," *IET Microw., Antennas Propag.*, vol. 10, no. 5, pp. 546–552, 2016.
- [37] M.-Y. Li *et al.*, "Eight-port orthogonally dual-polarized antenna array for 5G smartphone applications," *IEEE Trans. Antennas Propag.*, vol. 64, no. 9, pp. 3820–3830, Sep. 2016.
- [38] Y.-L. Ban, C. Li, C.-Y.-D. Sim, G. Wu, and K.-L. Wong, "4G/5G multiple antennas for future multi-mode smartphone applications," *IEEE Access*, vol. 4, pp. 2981–2989, 2016.
- [39] S.-H. Chang and W.-J. Liao, "A novel dual band circularly polarized GNSS antenna for handheld devices," *IEEE Trans. Antennas Propag.*, vol. 61, no. 2, pp. 555–562, Feb. 2013.
- [40] W.-J. Liao, J.-T. Yeh, and S.-H. Chang, "Circularly polarized chip antenna design for GPS reception on handsets," *IEEE Trans. Antennas Propag.*, vol. 62, no. 7, pp. 3482–3489, Jul. 2014.
- [41] Z. Zahid, L. Qu, H.-H. Kim, and H. Kim, "Circularly polarised loop-type ground radiation antenna for mobile devices using a resonance inductor and capacitor," *Electron. Lett.*, vol. 54, no. 5, pp. 262–264, Mar. 2018.
- [42] Z. Liang, Y. Li, and Y. Long, "Multiband monopole mobile phone antenna with circular polarization for GNSS application," *IEEE Trans. Antennas Propag.*, vol. 62, no. 4, pp. 1910–1917, Apr. 2014.
- [43] K. O. Gyasi *et al.*, "A compact broadband cross-shaped circularly polarized planar monopole antenna with a ground plane extension," *IEEE Antennas Wireless Propag. Lett.*, vol. 17, no. 2, pp. 335–338, Feb. 2018.
- [44] Y. Yao, X. Wang, X. Chen, J. Yu, and S. Liu, "Novel diversity/MIMO PIFA antenna with broadband circular polarization for multimode satellite navigation," *IEEE Antennas Wireless Propag. Lett.*, vol. 11, pp. 65–68, 2012.
- [45] L. Qu, H. Piao, Y. Qu, H.-H. Kim, and H. Kim, "Circularly polarised MIMO ground radiation antennas for wearable devices," *Electron. Lett.*, vol. 54, no. 4, pp. 189–190, Feb. 2018.
- [46] L. Qu, Z. Zahid, H.-H. Kim, and H. Kim, "Circular polarized ground radiation antenna for mobile applications," *IEEE Trans. Antennas Propag.*, vol. 66, no. 5, pp. 2655–2660, May 2018.
- [47] R. F. Harrington and J. R. Mautz, "Theory of characteristic modes for conducting bodies," *IEEE Trans. Antennas Propag.*, vol. AP-19, no. 5, pp. 622–628, Sep. 1971.
- [48] M. F. Abedin and M. Ali, "Modifying the ground plane and its effect on planar inverted-F antennas (PIFAs) for mobile phone handsets," *IEEE Antennas Wireless Propag. Lett.*, vol. 2, pp. 226–229, 2003.

- [49] C.-H. Chang and K.-L. Wong, "Bandwidth enhancement of internal WWAN antenna using an inductively coupled plate in the small-size mobile phone," *Microw. Opt. Technol. Lett.*, vol. 52, no. 6, pp. 1247–1253, Jun. 2010.
- [50] S.-W. Su and T.-C. Hong, "Radiation improvement of printed, shorted monopole antenna for USB dongle by integrating choke sleeves on the system ground," *IEEE Trans. Antennas Propag.*, vol. 59, no. 11, pp. 4383–4388, Nov. 2011.
- [51] L. Qu, R. Zhang, H. Shin, J. Kim, and H. Kim, "Performance enhancement of ground radiation antenna for Z-wave applications using tunable metal loads," *Electron. Lett.*, vol. 52, pp. 1827–1828, Oct. 2016.
- [52] Y. Liu, H.-H. Kim, and H. Kim, "Loop-type ground radiation antenna for dual-band WLAN applications," *IEEE Trans. Antennas Propag.*, vol. 61, no. 9, pp. 4819–4823, Sep. 2013.
- [53] L. Qu, R. Zhang, H. Lee, and H. Kim, "Compact triple-band ground radiation antenna using two inner rectangular loops enclosed by two outer loops," *Electron. Lett.*, vol. 52, no. 10, pp. 790–792, May 2016.
- [54] L. Qu, R. Zhang, and H. Kim, "High-sensitivity ground radiation antenna system using an adjacent slot for Bluetooth headsets," *IEEE Trans. Antennas Propag.*, vol. 63, no. 12, pp. 5903–5907, Dec. 2015.
- [55] H. H. Park, "Reduction of electromagnetic noise coupling to antennas in metal-framed smartphones using ferrite sheets and multi-via EBG structures," *IEEE Trans. Electromagn. Compat.*, vol. 60, no. 2, pp. 394–401, Apr. 2018.
- [56] H. Wang, V. Khilkevich, Y.-J. Zhang, and J. Fan, "Estimating radio-frequency interference to an antenna due to near-field coupling using decomposition method based on reciprocity," *IEEE Trans. Electromagn. Compat.*, vol. 55, no. 6, pp. 1125–1131, Dec. 2013.



Longyue Qu (M'18) was born in Handan, China, in 1990. He received the B.S. degree in electronic engineering from Yanbian University, Yanbian, China, in 2013, and the M.S. and Ph.D. degrees in electromagnetics and microwave engineering from Hanyang University, Seoul, South Korea, in 2015 and 2018, respectively.

His current research interests include antenna theory and design for mobile communications, metamaterial-based antenna technology, millimeter-wave arrays, and RF circuits.

Dr. Qu serves as a reviewer for several international journals, such as the *IEEE TRANSACTIONS ON ANTENNAS AND PROPAGATION*, the *IEEE ANTENNAS AND WIRELESS PROPAGATION LETTERS*, the *IEEE ACCESS*, *IEEE Antennas and Propagation Magazine*, the *Electronics Letters*, and the *ETRI Journal*.



Hyeongdong Kim (M'97) received the B.S. and M.S. degrees from Seoul National University, Seoul, South Korea, in 1984 and 1986, respectively, and the Ph.D. degree from the University of Texas at Austin, Austin, TX, USA, in 1992.

From 1992 to 1993, he was a Post-Doctoral Fellow with the University of Texas at Austin. Since 1993, he has been a Professor with the Department of Electrical and Computer Engineering, Hanyang University, Seoul. His current research interests include antenna theory and design especially for mobile

devices, e.g., wideband, high efficiency, multiband, multi-in multi-output, and high sensitivity.